A POINT-MASS MODEL OF GIBBON LOCOMOTION

JOHN E. A. BERTRAM[1],*, ANDY RUINA[2], C. E. CANNON[3], YOUNG HUI CHANG[4]
AND MICHAEL J. COLEMAN[5]

[1]College of Veterinary Medicine, Cornell University, USA, [2]Theoretical and Applied Mechanics, Cornell University, USA, [3]Sibley School of Mechanical and Aerospace Engineering, Cornell University, USA, [4]Department of Integrative Biology, University of California-Berkeley, USA and [5]Sibley School of Mechanical and Aerospace Engineering, Cornell University, USA

*Author for correspondence at Department of Nutrition, Food and Exercise Sciences, 436 Sandels Building, Florida State University, Tallahassee, FL 32306, USA (e-mail: jbertram@garnet.acns.fsu.edu)

Summary

In brachiation, an animal uses alternating bimanual support to move beneath an overhead support. Past brachiation models have been based on the oscillations of a simple pendulum over half of a full cycle of oscillation. These models have been unsatisfying because the natural behavior of gibbons and siamangs appears to be far less restricted than so predicted. Cursorial mammals use an inverted pendulum-like energy exchange in walking, but switch to a spring-based energy exchange in running as velocity increases. Brachiating apes do not possess the anatomical springs characteristic of the limbs of terrestrial runners and do not appear to be using a spring-based gait. How do these animals move so easily within the branches of the forest canopy? Are there fundamental mechanical factors responsible for the transition from a continuous-contact gait where at least one hand is on a hand hold at a time, to a ricochetal gait where the animal vaults between hand holds? We present a simple model of ricochetal locomotion based on a combination of parabolic free flight and simple circular pendulum motion of a single point mass on a massless arm. In this simple brachiation model, energy losses due to inelastic collisions of the animal with the support are avoided, either because the collisions occur at zero velocity (continuous-contact brachiation) or by a smooth matching of the circular and parabolic trajectories at the point of contact (ricochetal brachiation). This model predicts that brachiation is possible over a large range of speeds, handhold spacings and gait frequencies with (theoretically) no mechanical energy cost. We then add the further assumption that a brachiator minimizes either its total energy or, equivalently, its peak arm tension, or a peak tension-related measure of muscle contraction metabolic cost. However, near the optimum the model is still rather unrestrictive. We present some comparisons with gibbon brachiation showing that the simple dynamic model presented has predictive value. However, natural gibbon motion is even smoother than the smoothest motions predicted by this primitive model.

Key words: gibbon, ricochetal locomotion, brachiation, point-mass model.

Introduction

The swinging motion seen when brachiators move beneath their overhead supports naturally brings to mind the oscillations of a pendulum and the repeated interchange of gravitational potential energy (E_p) with kinetic energy (E_k). It is tempting, then, to assume that brachiating apes use natural pendular motions to reduce the muscular investment necessary to travel within the forest canopy (Ashton and Oxnard, 1964a,b; Fleagle, 1974; Preuschoft and Demes, 1984). Previous pendular swinging models are all based explicitly or implicitly on a half cycle of a freely swinging pendulum.

Under some circumstances, brachiators do move roughly according to the predictions of simple oscillatory pendular motion. Preuschoft and Demes (1984) modeled brachiation as a distributed-mass simple pendulum. They found good agreement with observed brachiation in gibbons for relatively slow brachiation. They predicted a natural pendular period of 0.98 s, while empirically measured periods in similar sized gibbons ranged from 0.83 to 0.95 s for slow, continuous-contact brachiation. Some limitations in the pendular swinging models have been attributed to model oversimplification with regard to both poor representation of the complex mass distribution of the animal and potential movements of non-support limbs during the swing (Fleagle, 1974; Preuschoft and Demes, 1984). Swartz (1989) pointed to the narrow range in oscillation frequency that pendular swinging models allow. Preuschoft and Demes (1984) recognized many of the features affecting ricochetal brachiation (see their Fig. 12.5), but the pendular model they presented did not calculate any

predictions for the more athletic ricochetal brachiation maneuvers of gibbons.

Gibbons display two brachiation gaits. At slower rates of forward progression, the gibbon uses a continuous-contact gait that is characterized by a dual-limbed support phase during a stride cycle. As in human walking, the duty factor of each limb is ⩾0.5 and there is always at least one limb in contact with the overhead support. At higher forward velocities the animal uses a ricochetal brachiation gait that is characterized by a non-contact phase between support phases of each step (the step is defined here as the period from hand contact to the next contralateral hand contact).

Here we describe a simple model which extends the pendular continuous-contact models in a simple way for gibbon ricochetal brachiation. With this mechanism, step periods can be arbitrarily long or short, even with a given pendulum length.

Continuous contact and ricochetal point-mass models

In the simplest rendition of the pendular swinging model, brachiation is viewed as a sequence of half-cycle motions of a simple point-mass pendulum. In this model, the center of mass moves along a sequence of circular arcs (Fig. 1A). If friction and elasticity are neglected, the system can continue its motion without investment of energy above that necessary to place the next supporting arm into the appropriate position for the following step. In this system, no energy is lost in the interactions of the system with its support because collisional losses are eliminated by the motion coming to a rest at the end of each arc. Hence the swing period is a half cycle of a simple pendulum. Higher frequency motions are imaginable but require energy supply to make up for collisional losses at the discontinuity as the center of mass changes direction at the transition from one circular arc to the next. In this paper, the only continuous-contact solutions we consider are those in which the center of mass (CM) comes to rest at the top of the swing when the change of hand holds occurs.

Like the ricochetal gait of a brachiator, the ricochetal model we propose utilizes a flight phase between hand contacts. We take the motion of the ricochetal brachiator to be a circular motion around the hand hold at full arm extension during support, combined with a parabolic free-flight arc between hand holds (Fig. 1B). We assume that the animal can coordinate its arms to have its hands in the proper place for each landing into a new circular arc around the next hand hold (limb mass is neglected in the model). In this model, collisional losses can again be reduced to zero by assuming that the gibbon chooses motions that make a smooth transition from the parabolic flight phase to the circular swing-support phase of the stride. That is, mechanically work-free motion of this model is possible if the tangent of the flight path during the flight portion of the stride is coincident with the arc of the swing as the animal begins the support portion of the stride (Fig. 1B, inset). Although this model appears to have a rather
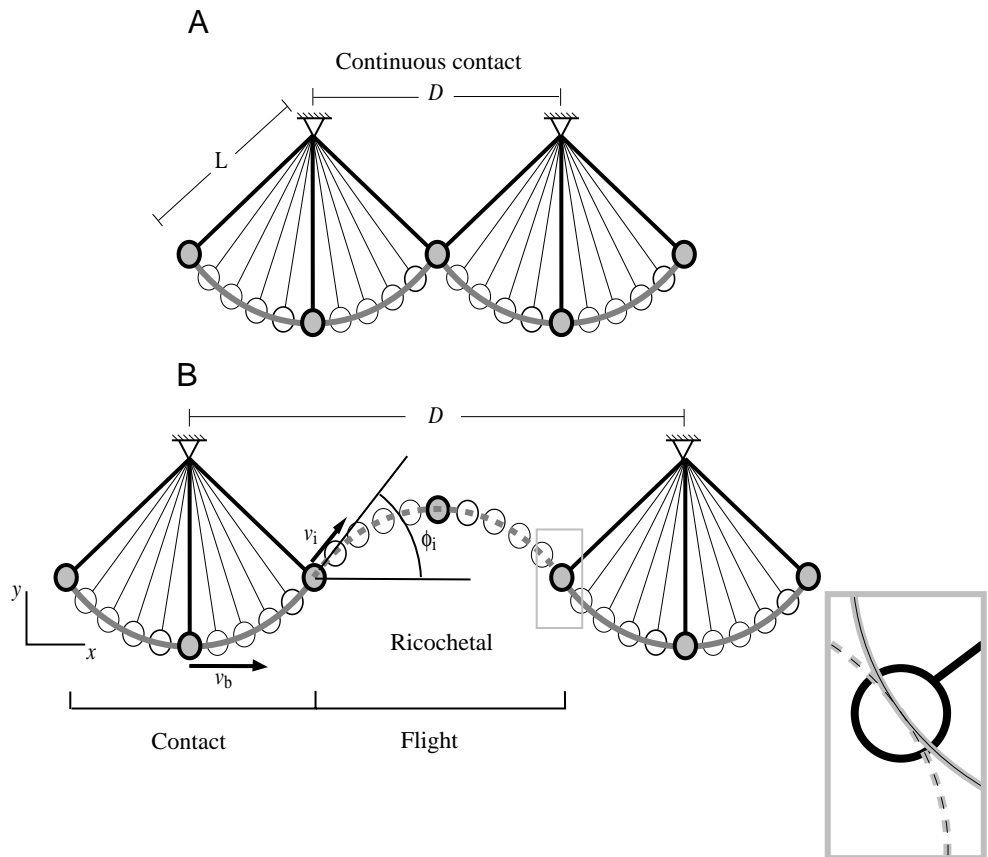

Fig. 1. Diagram of the model used. (A) The continuous-contact model in which there is no flight phase and the velocity is zero at the instant of double contact; (B) the two phases of the ricochetal model. The contact phase of the ricochetal model is similar to that of the continuous-contact model but the velocity is non-zero at the beginning and end of the swing phase. The flight phase between contacts is ballistic. The inset shows details of the transition from the parabolic arc of the flight phase to the circular arc of the swing phase. We assume that the trajectories are tangential at the transition. D, horizontal distance; L, length of massless inextensible link; v_b, maximum speed; v_i, speed at initiation of flight; ϕ_i, angle between pendulum and horizontal at initiation flight.

smooth motion, it does predict a discontinuity in acceleration and handhold reaction force when the ballistic flight phase begins and ends.

If the handhold spacing is less than twice the arm length, then both the continuous contact and ricochetal modes of mechanically cost-free transport are available. These models, together, are essentially equivalent to the minimal-biped model of Alexander (1995) turned upside down. These models cannot quite be classified with the passive-dynamic locomotion models of the types recently investigated for walking (e.g. McGeer, 1990; Garcia et al., 1998) because, as for the swinging leg in Alexander's minimal-biped model, the non-contacting arm in this minimal-bimanual model is assumed to be appropriately coordinated by a conscious (non-passive) controller. This two-dimensional point-mass model is probably the simplest model that could feasibly provide useful information about the dynamics of gibbon brachiation.

Governing equations

The brachiator is modeled as a massless inextensible link with length L connected to a point mass m. As a guess for comparison with data, L represents the distance from the animal's CM to the hand grip when hanging (this definition might slightly contradict another possibly useful definition of L as half the distance between the most distant objects the animal can simultaneously hold). We want to track the position of the center of mass (x, y) in time t as the animal moves from one hand hold to the next, a horizontal distance D away. While swinging, the pendulum makes an angle ϕ with the horizontal until the initiation of flight at ϕ_i. The speed v has a maximum speed v_b at the bottom of pendular swing arc when the tension in the pendulum is also at its maximum T_b. The speed at the initiation of flight is v_i, and the average horizontal speed is $v_{av}=D/t_{tot}$ where $t_{tot}=t_c+t_f$ and t_c and t_f are the pendular contact time and the flight time, respectively. The total, potential and kinetic energies are E, E_p and E_k, respectively. We denote differentiation with respect to time by superposed dots.

In the pendular contact phase, motion is governed by the simple pendulum equation. During flight we have the standard ballistics equations:

$$\ddot{\phi} + \frac{g}{L}\sin\phi = 0 \qquad (1)$$

for the pendular (contact) phase and

$$\ddot{y} = -g \quad \text{and} \quad \ddot{x} = 0 , \qquad (2)$$

for the flight phase, where g is the acceleration due to gravity.

Assuming no velocity discontinuities and hence no collisional losses, the trajectory is left-right symmetric about both the bottom of the pendulum swing and the top of the flight parabola. Note, again, that acceleration and force are necessarily discontinuous at the transition from swing to flight and from flight to swing.

For most calculations, we assume a value for the handhold spacing D and takeoff angle ϕ_i and calculate other quantities of interest as follows. Since the flight time is $t_f=2[(v_i\sin\phi_i)/g]$

and the horizontal component of flight velocity is $v_i\cos\phi_i$, Fig. 1B shows that

$$D/2 = L\sin\phi_i + [(v_i\sin\phi_i)/g]v_i\cos\phi_i , \qquad (3)$$

in which we can solve for v_i in terms of D, L and ϕ_i. Energy conservation

$$E = mv_b^2/2 = (mv^2/2) + mgy \Rightarrow v_i^2 = v_b^2 + 2gL(\cos\phi_i - 1) \quad (4)$$

then tells us the value of the maximum speed v_b and hence the maximum tension $T_b=m(g+v_b^2/L)$. That is, for a given m, g and L, the same motion that minimizes total energy also minimizes the peak arm tension. Energy balance also yields the angular velocity as a function of angle, from which we can calculate exactly the pendular contact time as

$$\frac{t_c}{\sqrt{L/g}} = \sqrt{2} \int_0^{\phi_i} \frac{d\phi}{\sqrt{[E/(mgL)] + \cos\phi - 1}} \qquad (5)$$

or approximately as

$$\frac{t_c}{\sqrt{L/g}} \approx \frac{2}{c} \sin^{-1}\left(\frac{c\phi_i}{\sqrt{2E/mgL}}\right) , \qquad (6)$$

where

$$c = \frac{\sqrt{2(1 - \cos\phi_i)}}{\phi_i} \quad \text{and} \quad \sqrt{2} \approx 1.41 . \qquad (7)$$

Although the exact integral (equation 5) can be expressed in terms of elliptic integrals, we chose to use a simple numerical quadrature (quad8.m in MATLAB®) for evaluation. The approximation in equation 6 is based on modeling the pendulum as a linear torsional oscillator with effective torsional stiffness $(mg/L^2)/c^2$ and thus the same energy as a gravitational pendulum at ϕ_i. This approximation turns out to be accurate within 1% or less for angles up to 90° and all energies except when D is close to $2L$ and the flight initiation angle is more than about 60°. In the worst exceptional case, the error in t_c is approximately 5%. Thus, with a loss of accuracy that is far less than our other modeling approximations, it is possible to use the approximate formula equation 6 for the contact time, making our model fully closed form. None of our general predictions depend on which of equations 5 or 6 are used. We can now calculate a variety of simple kinematic quantities. As a check, and in order to prepare for more elaborate models, we have also calculated these quantities by numerically integrating the equations of motion, equations 1 and 2.

The first of equations 4 applied at flight initiation $\phi=\phi_i$ determines the total energy as:

$$E = mgL\left[\frac{1}{2}\left(\frac{v_i}{\sqrt{gL}}\right)^2 - \cos\phi_i + 1\right]. \qquad (8)$$

Note that the continuous-contact pendular swinging

brachiation model is a subset of the ricochetal brachiation model described above but with $v_i=0$ and $t_f=0$.

For a given handhold spacing there are a number of different solutions of the center of mass trajectories, as shown to scale in Fig. 2, in this case with $D=4L$. In Figs 3A–D, 4A, various motion quantities are shown for families of solutions. The extremes of these solutions are obviously beyond the capabilities of an animal for a variety of reasons. From these solutions we can make the following observations. (1) For a given handhold spacing greater than $2L$, there are high energy ricochetal solutions for both low and high flight initiation angles (Figs 2, 3C). (2) At $2L\sin\phi_i=D$, the ricochetal solution matches the continuous-contact swinging solution. (See Fig. 3A, for example.) (3) For handhold spacings of less than $2L$, there are ricochetal solutions only so long as $2L\sin\phi_i<D$. In Fig. 3A, for example, the solutions at a given $D<2L$ have a maximum ϕ_i where they meet the continuous-contact solution. (4) For $D<2L$ contact time t_c is an increasing function of flight initiation angle, but is always less than the period of a simple pendulum with the same amplitude motion (i.e. the continuous-contact solution). (5) For all but the nearly continuous-contact motions, the contact time in ricochetal motion is less than the period of a linearized simple pendulum (π in the dimensionless plot of Fig. 3A). But the flight phase is arbitrarily long, so there are no fundamental restrictions on stride period for a given hand spacing greater than $2L$ (see Fig. 3B). (6) The average forward speed is seen to be highest at small flight initiation angles where the flights are more flat (Fig. 3D).

Optimization criteria

In order to reduce the range of possible solutions that satisfy our general criteria (i.e. tangency of the swing arc and flight parabola), one would like to define an optimization criterion. The most obvious optimization criterion is the specific energetic cost of transport (energy used per unit weight per unit distance). However, this measure is already optimal (at 0) for all the solutions shown. None of the motions considered require any energy input, at least theoretically. Another candidate for optimization is speed; however, the model allows arbitrarily high speeds (the low trajectories in Fig. 2, corresponding to small ϕ_i in Fig. 3D, are the fast ones). Thus, we need to seek a more subtle candidate for the optimization. For an animal that does not want to waste energy starting, stopping or changing gaits, we might seek minimum total energy solutions. Note that, in Fig. 2, the low, fast solutions (small ϕ_i) have high total energy as do the high, looping (large ϕ_i) solutions (see Fig. 3C) for $D>2L$. Also, it is likely to be advantageous for an animal to reduce the force demands on its muscles or bones or to reduce stress. As noted, the solution that minimizes the total energy of the system is also the one that minimizes the maximum tensile force in the supporting arm. Thus, we can tentatively make more definitive predictions about the model by picking an 'optimal' motion from amongst the range of possible motions. Fig. 3C shows the total energy of some solutions at various values of D, as a function of the take-off angle ϕ_i. As can be seen in Fig. 3C and can be shown by differentiation of the equations above, the optimal solution involves a flight initiation angle of $\phi_i=45°$ (so long as $D>\sqrt{2}L$). This choice of ϕ_i agrees with the classical ballistics intuition that the greatest range is achieved when a frictionless cannonball is launched at $45°$. [The set of parabolic trajectories of a fixed energy whose apex is on the y axis have an envelope made of two sloping $45°$ sloping angles. Finding the lowest energy trajectory is equivalent to sliding the apex of this wedge up to the lowest point where the envelope matches the boundary conditions, i.e. either the launch and land points (from classical ballistics) or the launch and land circles (from the ricochetal oscillation model).]

Even though the mechanical energy is minimized by a flight initiation angle of $45°$, the total mechanical energy of the model is within 20 % of this optimum for flight initiation angles from $32°$ to $62°$. Thus, we cannot treat the optimization criterion as one that would tightly constrain behavior, given that other quantities we have neglected likely need to be controlled and optimized by an animal as well.

The primary metabolic cost of locomotion may be for turning on and off muscle force and not for doing work, as proposed for running by Kram and Taylor (1990). If the
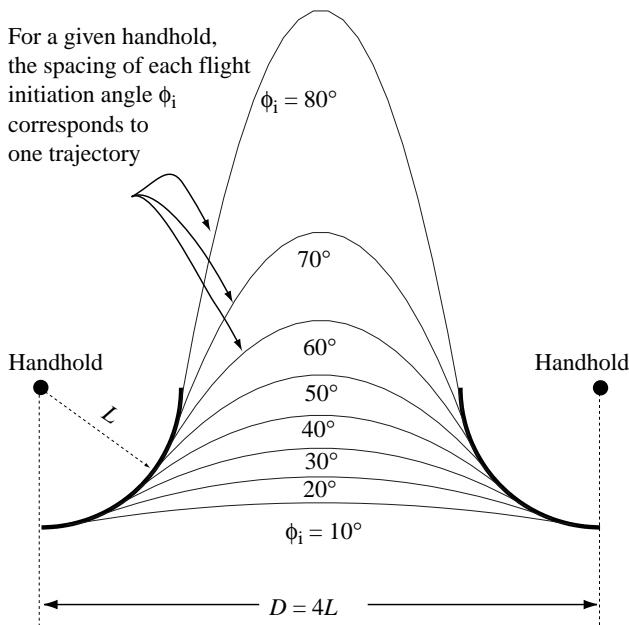

Fig. 2. Various trajectories that satisfy the requirement that the swing and flight trajectories be coincident at the transition between the two. Each of the flight paths shown is no-collision and no-loss. The family of trajectories depicted is for a single handhold spacing. For high flight initiation angles, e.g. $\phi_i=80°$, the energy of the motion is high, the average forward speed is low, and the peak tension in the arms is high. For low flight initiation angles, e.g. $\phi_i=10°$, the energy is again high, as are average forward speed and peak arm tension. A portion of the circular arc of the swing trajectory is shown by the heavy line at each end of the parabolic flight trajectory. The relationship between various motion quantities, handhold spacing D and flight initiation angle ϕ_i is shown in Fig. 3. L, length of massless inextensible link.
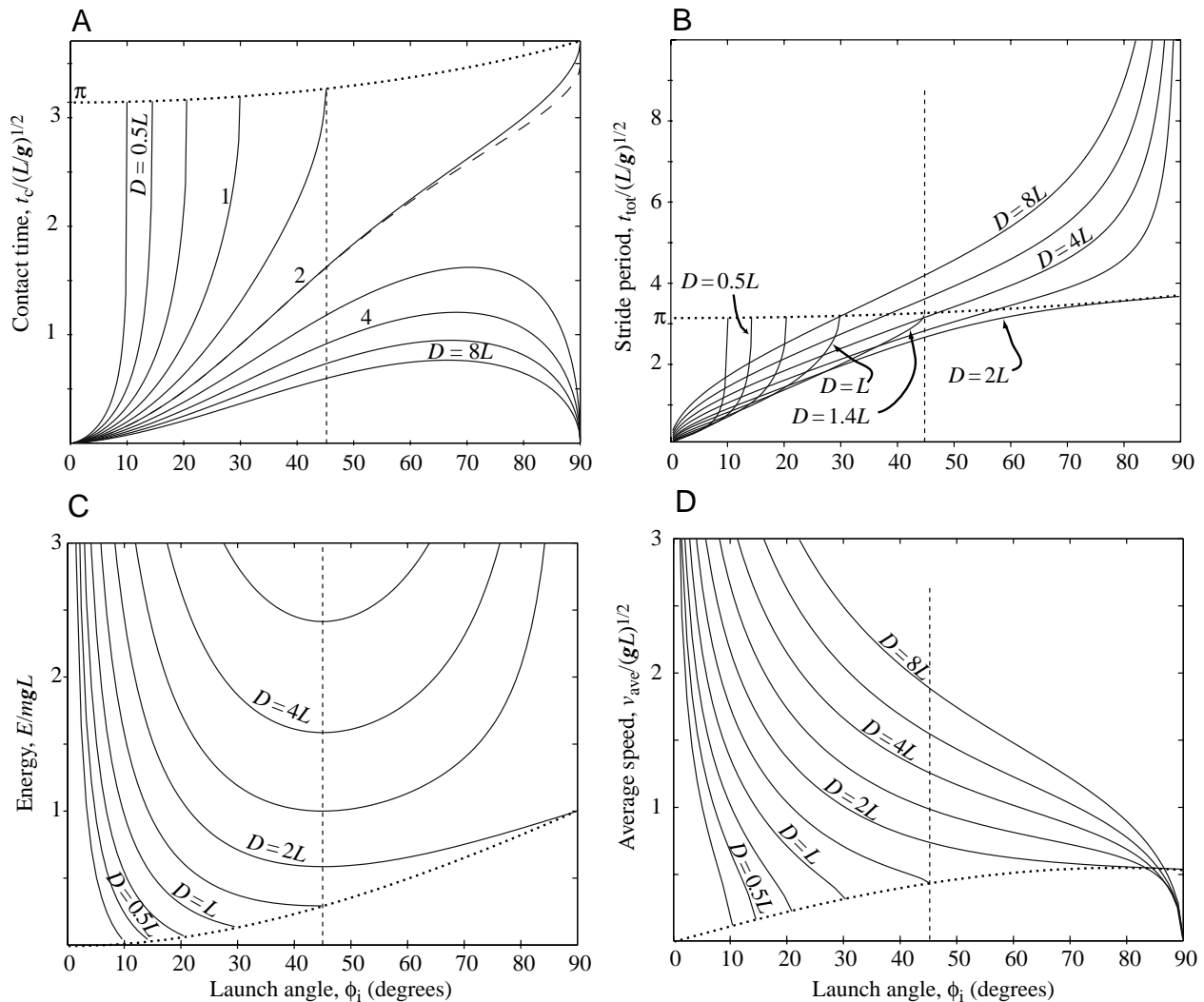
Fig. 3. Various point-mass model predictions for both continuous-contact (dotted lines; $D=2L\sin\phi_i$) and ricochetal (solid lines) motions as a function of flight initiation angle ϕ_i. In A–D, the solid curve represents predictions for one handhold spacing D. Ten values of D are shown varying by the ratio of $\sqrt{2}$. The dotted lines show the solutions for continuous contact in which D determines ϕ_i. The maximum D for continuous contact is $2L$. For $D\leqslant 2L$, where L is the length of the massless inextensible link, the ricochetal model terminates where it meets the continuous-contact model (continuous contact is then the same as ricochetal with no flight phase). (A) Contact time (t_c), the time from hand contact to release. Note that the continuous-contact model predicts a contact time that is always close to that predicted by the period of small oscillations of a simple pendulum, $t_c=\pi\sqrt{(L/g)}$. An analytical approximation (dashed line; described in the text) is almost indistinguishable from the (exact) numerical solution except when L is approximately 2 and for flight initiation angles over approximately 70°. (B) The time of one 'step', including contact and ballistic phases (t_{tot}). In the ricochetal model, all periods are possible, from zero to infinity. In the continuous-contact model, the periods are the same as those in A and range only from approximately 3.14 to 3.9. (C) The total mechanical energy E of the motion, which is also the kinetic energy at the bottom of the swing phase. For $D\leqslant\sqrt{2}L$, the energy is minimal for a launch angle of $\phi_i=45°$. A minimum in energy also corresponds to a minimum in the peak tension in the arms. Note, however, that this minimum is broad so it is approximately reached for a range of ϕ_i. (D) Average horizontal speed (v_{ave}) of the centre of mass. For continuous-contact motion, the forward speed tends to zero as the swing angle tends to zero. For ricochetal motion, the forward speed becomes arbitrarily large as the flight initiation angle ϕ_i tends to zero. As the flight initiation angle tends to 90°, the ballistic time becomes large (the difference between B and A is the ballistic time) and average forward motion is slow.

metabolic cost of gaining a momentary isometric tension is proportional to the magnitude of tension in the support limb and roughly independent of time, the metabolic cost per unit distance of transport would be proportional to peak tension divided by the distance between contractions D. This measure of 'cost' (see Fig. 4A) also has a minimum at $\phi_i=45°$. This

minimum is also broad so the cost function is nearly optimized for a large range of flight initiation angles. Surprisingly, this cost is almost independent of handhold spacing (the curves in Fig. 4A nearly fall on top of each other).

Finally, if we accept $\phi_i=45°$ as the preferred ricochetal mode, since it minimizes energy, peak arm tension and 'cost',
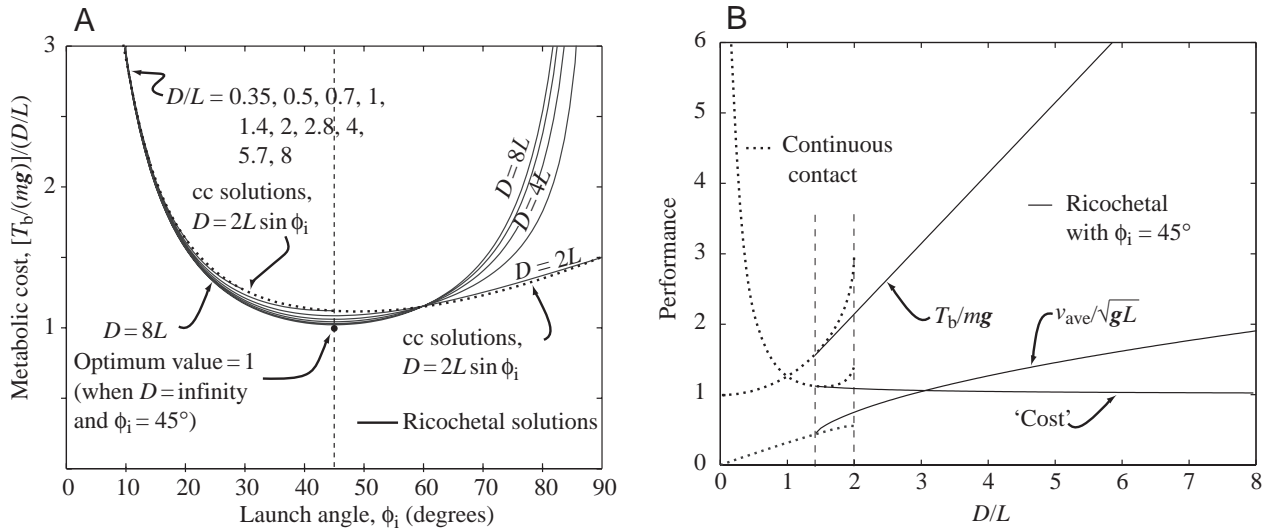
Fig. 4. (A) A measure of the metabolic cost is the peak tension required per distance traversed. Note that for any value of D, the distance between hand holds, this cost is minimized by a flight initiation angle ϕ_i of 45° and is nearly reached for any D and any launch angle ϕ_i in the range of 30° to 60°. (B) A comparison of the performance of the continuous-contact (CC) model (dotted lines), and of the 'optimal' ricochetal model (solid lines) using $\phi_i=45°$ (the 'optimum' for energy and 'cost' from Figs 3C, 4A) as a function of handhold spacing. Three measures of performance are shown: peak tension (T_b/mg), 'metabolic cost' from Fig. 4A, and average speed ($v_{ave}/\sqrt{gL}$). At $D=\sqrt{2}L$, the continuous-contact and ricochetal solutions are the same. For $D<\sqrt{2}L$, there is no $\phi_i=45°$ ricochetal solution, and the lowest cost and lowest peak tension ricochetal solutions are the ones that have vanishing ballistic phase (i.e. are identical to the continuous-contact solution). For $D>2L$, there is no continuous-contact solution.

we can look at various measures of performance for continuous-contact motion and for 'optimal' ricochetal motion, as shown in Fig. 4B. Shown are peak tension (the total energy curve would be similar), average speed and the 'cost' function described above. Tension and energy are minimized by arbitrarily small handhold spacings but average speed and 'cost' both favor arbitrarily large handhold spacings.

Limited reach alone, as determined by extended arm length, demands a transition to ricochetal motion for handhold spacings $D>2L$. But ricochetal motions are possible for arbitrarily small handhold spacings. The three optimal conditions discussed all predict that the (barely) ricochetal motion corresponding to continuous-contact motion is best for handhold spacings less than $\sqrt{2}L$ and that ricochetal solutions are preferred for larger spacings. In Fig. 4B, the continuous-contact solutions are shown within the band that corresponds to $\sqrt{2}L<D<2L$, even though they are not optimal there. The figure makes evident that a gibbon would suffer little penalty for any of the three optimal criteria for delaying that transition until at least about 1.7L. Such a gait-transition delay would postpone the obvious decrease in security and maneuverability caused by losing hand contact.

The dynamics of gibbon brachiation

In order to determine how well the model described above, either restricted by the optimization criterion or not, corresponds to the brachiation behavior of a gibbon, we compared some of the predictions of the model with measurements of the brachiation in a 7.95 kg female White-handed gibbon (*Hylobates lar*). The techniques utilized to make

these measurements are fully described in Chang et al. (1997). Briefly, a universal force transducer of our own design was mounted to the ceiling of a reinforced chain-link exercise cage of dimensions 3.71 m wide, 6.10 m long and 3.56 m high. Uninstrumented hand holds identical to that of the transducer were also mounted to the ceiling of the exercise cage in series with the transducer hand hold. The distance between hand holds for different analysis sessions was adjusted to be at equal intervals of either 0.8, 1.2, 1.6, 1.72, 1.95 or 2.25 m. The number of hand holds was maximum at seven (the instrumented transducer in the center of six non-instrumented hand holds) and minimum at three (the transducer flanked by two non-instrumented hand holds). The cage restricted the number of hand holds for longer spacings; at these longer distances the animal always used ricochetal brachiation. Only those runs in which the change in horizontal velocity was small were used in this analysis, as determined by integration of the horizontal load. A lateral video image was taken (60 Hz, 1/500 s shutter speed) as the animal brachiated freely across the hand holds.

Time of contact with the hand hold for a given run was determined from the force transducer output. Contact with the transducer was easily determined and was accurate to 5 ms, which was the channel sampling rate. Maximum and initial velocities were determined by integration of the force record after conversion to acceleration. Average forward velocity was determined from the calibrated video image. The video images of each run were digitized and the time and distance interval of a complete brachiation cycle was determined (NIH Image). This velocity value was used to determine the constant of integration for the horizontal motion from load cell data. The

constant was assumed zero in the vertical direction because the hand holds were all at the same height.

Results

Model predictions

Fig. 5 shows the relationship between average forward velocity and handhold spacing, comparing a brachiating gibbon with the model predictions. The model predicts two 'gaits': continuous-contact and ricochetal. At slower forward velocities and closer handhold spacing, the optimization criterion selects continuous-contact gait, in which at least one hand is in contact with the hand hold at all times. The model is then just a sequence of simple pendulum motions placed side by side. At higher forward velocities and for handhold spacings with $D > \sqrt{2L}$, the optimization criterion selects the ricochetal solution with a flight initiation angle of $45°$ (the theoretical portions of Fig. 5 duplicate the v_{ave} curve in Fig. 4B).

The time course of the vertical and horizontal forces predicted by the model and measured in a brachiating gibbon is illustrated in Fig. 6. The fluctuations of force are much smoother in the gibbon compared with the model. The model underestimates the peak vertical force, although the net impulse is similar.
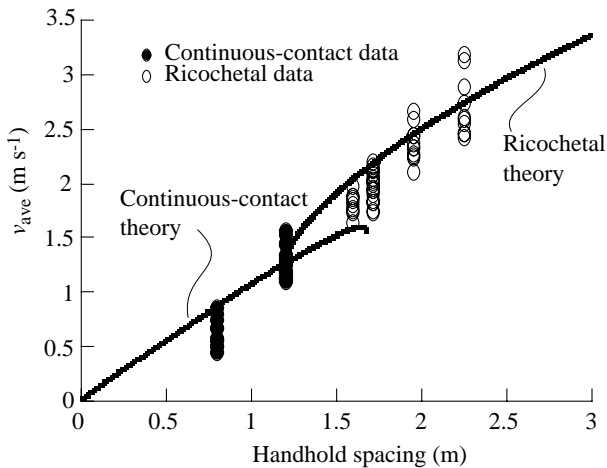

Fig. 5. Relationship between handhold spacing (D) and average forward velocity (v_{ave}) for the computational model and for a freely brachiating gibbon. The two theoretical curves are the continuous-contact and 'optimal' ricochetal curves marked v_{ave} reproduced from Fig. 4B. Brachiation steps for a gibbon are shown as filled (continuous contact) and open circles (ricochetal). Minimization of energy, peak tension or 'cost' predicts a gait transition at $D = \sqrt{2L}$, where D is the ditance between hand holds and L is the distance from the animal's center of mass to the hand hold. One of the handhold spacings is just larger than that and is consistently chosen by the gibbon as continuous contact, and is thus very slightly suboptimal by the primitive criteria considered here. The next larger handhold spacing does allow both ricochetal and continuous-contact solutions, and the gibbon always uses the ricochetal solution. This may not be surprising since the value of L we use in our model (0.84 m) is the distance from the hand to the center of mass, and the gibbon's arms and shoulders may not span the full distance (i.e. its half-shoulder spacing is probably smaller than the distance from the shoulder to the center of mass).
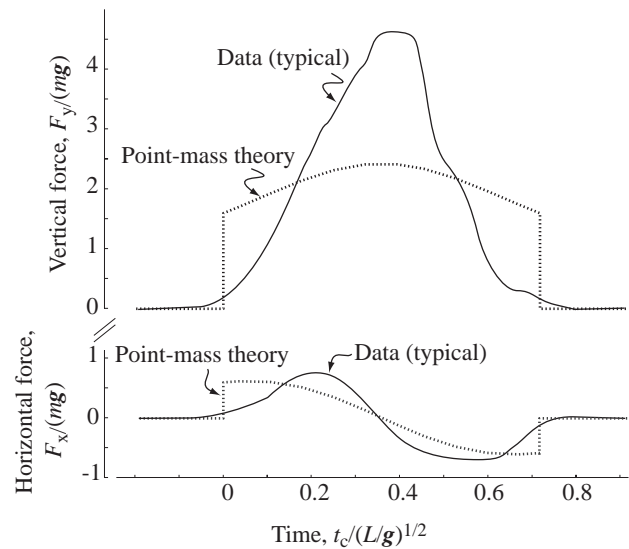

Fig. 6. Handhold force: theory and point-mass model, using mass m=7.96 kg with L=0.84 m, and a handhold spacing of D=2.25. The point-mass theory for flight initiation ϕ_i=45° is compared with a typical ricochetal data set. The approximate contact time (t_c) is well matched, as is the net impulse (area under the curves). The gibbon chooses a strategy that not only has no collisions, but also has smoothly varying force. Although the model was chosen to illustrate the lack of impulse at initial hand contact, the model is too simple to predict the extremely smooth grip of the gibbon.

Evaluating brachiation

There is substantial overlap between the prediction of the relationship between v_{ave} and handhold spacing of the model and the behavior observed in the brachiating gibbon (Fig. 5). The changeover from continuous-contact to ricochetal brachiation corresponds well between the model and observations. The model tended to overestimate v_{ave} except at the longest spacing of the continuous-contact gait (which corresponds to the changeover point of the two gaits) and the longer spacings of the ricochetal gait (1.9 and 2.25 m). Although the observed velocities do not differ significantly from the model's predictions (i.e. the model prediction lies within the 95 % confidence interval of velocities measured at each of the spacings), they are not adequate to fully evaluate the predictive capability of this model.

Although the theoretical prediction is as smooth as the model allows, the gibbon chooses an even smoother force profile (Fig. 6). This observation reinforces the notion that the avoidance of energy-dissipating inelastic collisions may be a key behavioral feature of brachiation. Smoothness of force transition is a way of further avoiding collision losses. The origin of the word 'jerk' for the time derivative of acceleration is probably due to the fact that, in systems with play or flexibility, a large rate of acceleration leads to internal collisions or internal motions. The gibbon, being actually more than a point mass, may well be avoiding such 'jerk' losses by maintaining a smooth force profile.

The simple pendulum and the ricochetal model motions we describe have some basic differences. This is the case even though they both swing below their support and the simple

pendulum represents a subset of the ricochetal solutions. One demonstration of this difference is indicated by the relationship between initial velocity of the body when it contacts the support and the maximum velocity it achieves during the swing. The simple pendulum model begins at an initial velocity of zero. The greater the arc of a pendulum (i.e. the larger the angle it swings through), the higher the velocity it will achieve at the bottom of the swing. Thus, for continuous contact, as support spacing or v_{ave} increases, the greater the difference between the v_i and v_b. This is in contrast to the ricochetal case. The ricochetal model makes contact with the support with a substantial v_i. The farther the handhold spacing or the faster the animal travels, the smaller the difference between v_i and v_b. In Fig. 7, the difference between v_b and v_i is plotted against v_{ave} for the pendulum and ricochetal models and for the gibbon brachiating in a continuous contact and ricochetal manner. Compared to the data, the simple point-mass model generally underestimates the velocity difference. However, continuous-contact brachiation shows a distinctive increasing trend that parallels the pendular prediction while ricochetal brachiation shows a decreasing trend that parallels the ricochetal prediction.

Time of hand contact (t_c) is a critical determinant of the interaction between the animal and its support. The time of contact is a measure of the time available for the limb's support musculature to be active and has been shown to correlate well with metabolic cost in terrestrial runners (Kram and Taylor, 1990). A plot of t_c against v_b has two distinctive predictions for the pendulum *versus* ricochetal motions (Fig. 7B). The maximum velocities v_b of the two models overlap substantially. The continuous-contact brachiation runs are scattered generally around the pendular model prediction, but the fit is not good. The behavior of the animal does not appear to be strongly influenced by the optimal pendular dynamics in continuous contact. However, the ricochetal runs are tightly grouped around the ricochetal prediction for these variables (Fig. 7B).

Discussion

The mechanics of brachiation have been conceptualized in the past exclusively as a simple pendulum (Andrews and Groves, 1976; Ashton and Oxnard, 1964a,b; Avis, 1962; Carpenter and Durham, 1969; Chivers, 1974; Fleagle, 1974; Jenkins et al., 1978; Jungers and Stern, 1984; Mittermeier, 1978; Parsons and Taylor, 1977; Preuschoft and Demes, 1984). When the pendulum model did not fulfill expectations, it was assumed that the details of the model did not adequately describe the complexities of the animal and its limbs, rather than questioning whether the pendular mechanism was an appropriate or adequate model of the behavior of these animals (Swartz, 1989). Our gibbon data indicate that only under limited circumstances is the movement of the gibbon determined by continuous-contact pendular mechanics. Even for continuous contact, the gibbon does not appear to be strongly restricted to the simple pendulum-like motions (Fig. 7).

Many aspects of our basic model match the model described by Preuschoft and Demes (1984), and it is interesting that many
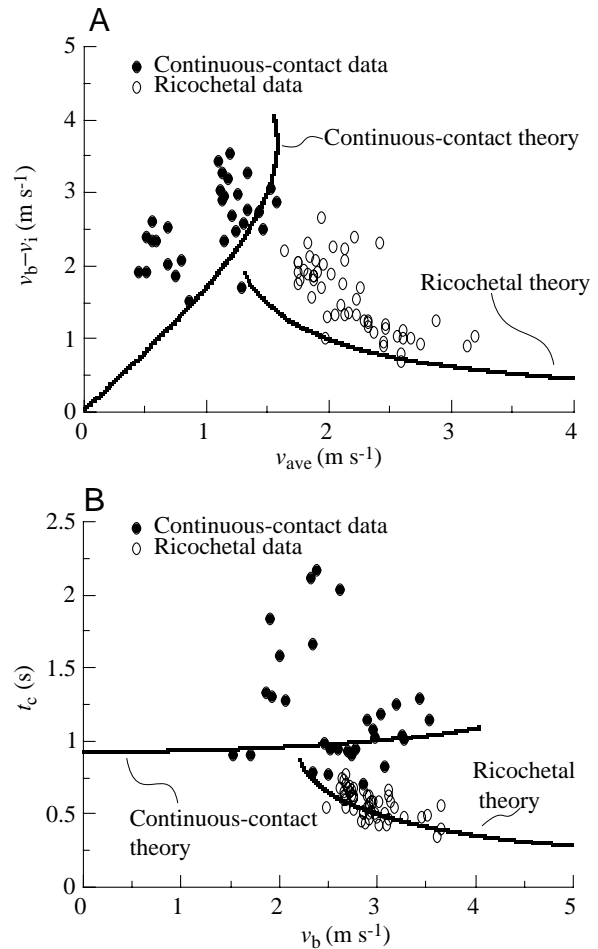

Fig. 7. Comparison of the point-mass model and gibbon brachiation. Model mass and arm length match that of the gibbon. The gibbon was allowed to brachiate freely across a series of equally spaced hand holds. The data set is composed of numerous runs at different handhold spacings. (A) The relationship between maximum velocity (v_b) of the swing and average forward velocity (v_{ave}). Point-mass model predictions of continuous-contact (left) and ricochetal brachiation (right) are shown by solid lines. Symbols indicate individual brachiation steps of a gibbon at a variety of handhold spacings; closed circles are continuous-contact steps and open circles are ricochetal steps. (B) The relationship between time of hand contact (t_c) and maximum velocity of the swing (v_b). Point-mass model prediction is the solid line above, ricochetal prediction is the solid line below. Symbols as in A. v_i, speed at flight initiation.

of their observations correspond with the quantitative results of our model. Preuschoft and Demes described the condition at the transition from the flight phase to the contact phase of the ricochetal stride that corresponds to the non-collision criterion we define. However, they did not define this condition as a critical criterion of ricochetal brachiation. They also did not identify optimization criteria or extend their model to quantify predicted ricochetal behavior.

Gibbons use ricochetal oscillations as a mechanism of bouncing between overhead hand holds in their higher velocity brachiation movements. Our simple model offers a solution to

the frequency restrictions associated with continuous-contact pendulum-based mechanisms. At the same time, the model offers a mechanism for minimizing energetic cost in brachiation. Theoretically, the ricochetal model is 100 % efficient, just as the continuous-contact pendular exchange and some models of running with springs.

In order to interpret the specialized morphological adaptations that characterize the brachiators, it is first necessary to determine the mechanical function(s) that their specific morphology allows. One major confusion that has obscured the interpretation of the anatomical specializations found in brachiators (limb and body proportions, joint anatomy, muscular activity and coordination, etc.) has been the misinterpretation of brachiation as primarily a pendulum-like movement. The data provided in this study show some evidence that, for ricochetal brachiation, the point-mass ricochetal model approximates both the scaling and trends in dynamic changes in locomotion. This is in spite of the model's gross oversimplification of the animal's complex morphology.

It must be recognized, however, that in the ricochetal gait the gibbon will not behave as a simple point-mass pendulum. Instead, the animal acts more like a jointed complex pendulum (J. E. A. Bertram and Y. H. Chang, submitted for publication). This difference likely accounts for some of the differences in the model's predictions and our direct measurements of gibbon brachiation (Figs 6, 7). Nevertheless, the trends described by our simple model clearly indicate that the gibbon is moving very much as we predict.

A feature of this model is the wide range of motions that it allows at near 'optimal' speeds. Gibbons appear to have developed a very simple, yet sophisticated strategy that allows them to maneuver at high velocity and change the distance between 'steps' with minimal energy loss. It is remarkably difficult for most terrestrial animals to arbitrarily alter the length of successive steps when running at high velocities, yet this is what is routinely demanded of the brachiator in its natural environment. Our model allows for a wide range of step lengths. Strategies based on this required functional flexibility may account for why brachiation is not such an economical mode of locomotion as our simplistic theory indicates it could be. For instance, based on analysis of oxygen consumption rates, it has been found in the neotropical spider monkeys *Ateles geoffroyi* and *A. belzebuth* that the cost of locomotion was always greater in brachiation *versus* quadrupedal walking (Parsons and Taylor, 1977).

Further analysis of the mechanics underlying brachiation will provide better understanding of the morphological specializations that have allowed brachiators to fully exploit their three-dimensionally complex environment. Brachiation may prove to be a fruitful area to investigate the quantitative relationship between functional morphospace and the adaptation of an integrated system to a complex locomotory task.

References

Alexander, R. M. (1995). Simple models of human motion. *Appl. Mech. Rev.* **48**, 461–469.

Andrews, P. and Groves, C. E. (1976). Gibbons and brachiation. In *Gibbon and Siamang*, vol. 4 (ed. D. M. Rumbaugh), pp. 167–218. Basel: Karger.

Ashton, E. H. and Oxnard, C. E. (1964a). Locomotion patterns in primates. *Proc. Zool. Soc. Lond.* **142**, 1–28.

Ashton, E. H. and Oxnard, C. E. (1964b). Function adaptations in the primate shoulder girdle. *Proc. Zool. Soc. Lond.* **142**, 49–66.

Avis, V. (1962). Brachiation: The crucial issue for man's ancestry. *Southw. J. Anthropol.* **18**, 119–148.

Carpenter, C. R. and Durham, N. M. (1969). A preliminary description of suspensory behavior in non-human primates. *Proc. 2nd Int. Congr. Primat.* **2**, 147–154.

Chang, Y. H., Bertram, J. E. A. and Ruina, A. (1997). A dynamic force and moment analysis system for brachiation *J. Exp. Biol.* **200**, 3013–3020.

Chivers, D. J. (1974). *The Siamang in Malaysia: A field study of a primate in a tropical rain forest.* Basel: Karger.

Fleagle, J. G. (1974). The dynamics of a brachiating siamang (*hylobates* [*symphalangus*] *syndactylus*). *Nature* **248**, 259–260.

Garcia, M., Chatterjee, A., Ruina, A. and Coleman, M. J. (1998). The simplest walking model: Stability, complexity, and scaling. *ASME J. Biomech. Eng.* **120**, 281–288.

Jenkins, F. A., Dombroski, P. J. and Gordon, E. P. (1978). Analysis of the shoulder in brachiating spider monkeys. *Am. J. Phys. Anthropol.* **48**, 65–78.

Jungers, W. L. and Stern, J. T. (1984). Kinesiological aspects of brachiation in lar gibbons. In *The Lesser Apes: Evolutionary and Behavioral Biology* (ed. H. Preuschoft, D. J. Chivers, W. Y. Brockelman and N. Creel), pp. 119–134. Edinburgh: Edinburgh University Press.

Kram, R. and Taylor, C. R. (1990). Energetics of running: a new perspective. *Nature* **346**, 220–221.

McGeer, T. (1990). Passive dynamic walking. *Intern. J. Robot Res.* **9**, 62–82.

Mittermeier, R. A. (1978). Locomotion and posture in *Ateles geoffroyi* and *Ateles paniscus*. *Folia Primatol.* **30**, 161–193.

Parsons, P. E. and Taylor, C. R. (1977). Energetics of brachiation versus walking: A comparison of a suspended and an inverted pendulum mechanism. *Physiol. Zool.* **50**, 182–189.

Preuschoft, H. and Demes, B. (1984). Biomechanics of brachiation. In *The Lesser Apes: Evolutionary and Behavioral Biology* (ed. H. Preuschoft, D. J. Chivers, W. Y. Brockelman and N. Creel), pp. 96–118. Edinburgh: Edinburgh University Press.

Swartz, S. M. (1989). Pendular mechanics and the kinematics and energetics of brachiating locomotion. *Int. J. Primat.* **10**, 387–418.

Swartz, S. M., Bertram, J. E. A. and Biewener, A. A. (1989). Telemetered in vivo strain analysis of locomotor mechanics of brachiating gibbons. *Nature* **342**, 270–272.

Taylor, C. R. (1994). Relating mechanics and energetics during exercise. *Sci. Comp. Med.* **38A**, 181–215.